A Framework for Fast Automatic Robot Ultrasound Calibration

Ruixuan Li*, Kenan Niu* and Emmanuel Vander Poorten

2021 International Symposium on Medical Robotics (ISMR) | 978-1-6654-0622-2/21/$31.00 ©2021 IEEE | DOI: 10.1109/ISMR48346.2021.9661495

***Abstract*— Ultrasound (US) has been increasingly used as medical imaging technology across various clinical diagnostic and therapeutic scenarios thanks to its availability and non-radiative nature. While 3D US probes are becoming available, most systems are still using 2D probes. For 3D US reconstruction based on 2D probes, US image calibration forms an essential step. Through calibration, one can find the transformation matrix between a coordinate frame attached to an optical marker or the robot's end effector towards the coordinate frame of the US probe. Current US calibration methods usually require hereto lengthy free hand gestures as well as some manual interventions, which hampers the use and integration with advanced robotic systems. This paper introduces a reliable automatic calibration framework that is also fast. Demonstrated on a KUKA lightweight robot and 2D US probe, the full calibration procedure was completed in 224.8 seconds with a 1.29 mm mean 3D localization error. Within this procedure, camera-to-robot calibration was accomplished within only 47 seconds and reached a 0.17 mm mean error. Validation of the US image calibration was done through 3D printed model, leading to a mean deviation of 1.05 mm from the respective CAD models.**

Keywords - Camera-to-robot calibration, KUKA, Robot control, US image calibration, 3D reconstruction

I. INTRODUCTION

Ultrasound (US) is widely and increasingly used in clinics for diagnosis and visualization during various therapies, e.g. to locate target tissue position [1], measuring movements of underlying tissues [2] or visualize 3D anatomical structures [3]. Unlike computed tomography (CT) causing ionizing radiation or magnetic resonance imaging (MRI) being very costly, US is non-radiative, portable and low-cost.

3D US reconstruction has received great attention in the past for it could allow clinicians to take three-dimensional structure of the anatomy better into account. Aside from expensive 3D probes, conventional techniques try to reconstruct 3D geometry by sweeping a 2D US probe over the patient while tracking the probe. In this context, the trajectory of the US probe is recorded together with corresponding US images for each frame.

Such a reconstruction approach has already been applied for US scanning systems for fetal anomalies [4], [5] and orthopedic surgery [6]. These studies clearly indicate the importance of accurate US calibration to obtain a good overall accuracy of 3D US reconstruction. Accurate spatial information of the US probe is needed for 3D US reconstruction. Optical, electromagnetic tracking or robot encoder and forward kinematics could be used. However, US poses cannot be directly measured from these methods. Dedicated calibration approaches are needed to provide an accurate transformation and calibration matrix.

In the past, several US calibration phantoms were designed with various geometry features [7]–[12]. Single cross wire phantom has been widely used for free hand US calibration. The cross point is aligned in US image plane and the center of intersection (cross point) is manually segmented for each image which makes it easy to prepare and conduct US image acquisition. This approach provides a reasonable result with root mean squared error (RMSE) from 1.4 mm to 3.2 mm [8]. However, manual segmentation procedure is time consuming and may introduce unwanted outliers that can affect the final accuracy of calibration algorithm. Sphere phantom is a variant that originates from the cross wire phantom where the center of sphere serves as cross-point [9]. The sphere contour produces a circular arc in US images. When the US image plane passes through the center of sphere, this feature thus can be used to automatically find the center in 2D US image. Multi wires phantom also originates from single cross wire phantom, but the manual US acquisition and image segmentation are still necessary and crucial steps. It may lead to inaccurate calibration outcomes [10]. Prager et al. proposed a new plane phantom with automatic image segmentation using edge detection and RANSAC line fitting [11]. Nevertheless, the US sweeping range is relatively large. Z-fiducial phantom is a fast calibration alternative using 'Z' configuration wires without requirement to align with target cross point [12]. Based on similar triangles theorem in Euclidean geometry, it is easy to compute the positions of intersection points on phantom coordinate frame. However, the scale factors can not be directly measured and need to be computed from other approaches [13]. Furthermore, commercial calibration phantoms (e.g. Model 040GSE, CIRS, Norfolk, VA) and devices provide an effective solution, but are quite expensive to be used in practice [14]. According to Hsu's review paper of different US image calibration methods, sphere phantom is easy to use for both experts and novices without complex training. This makes it easy for integration in a robotic system. Meanwhile, sphere phantom can offer the best precision and accuracy which is 0.59 and 1.77 mm, respectively [15]. In addition, free hand probe manipulation and image segmentation are usually time-consuming. The calibration process can take up to two hours depending on the number of acquired images [16]. Therefore, a rapid and automatic calibration procedure is required to reduce workload

* These authors contributed equally to this work.

R. Li, K. Niu and E. Vander Poorten are with the Department of Mechanical Engineering, KU Leuven, Belgium (email: kenan.niu@kuleuven.be)

This project has received funding from the European Union's Horizon 2020 research and innovation programme under grant agreement No. 101016985 and Flemish Research Foundation (FWO) under grant agreement No. G0A1420N.

and increase reproducibility. As such robot assisted US system could alleviate the uncertainty of free hand methods. Via 3D tracking system, the robot could also be linked to other surgical instruments and localized with respect to the patient to establish the spatial relation in same frame [17]–[19]. Next to US image calibration, a fast camera-to-robot calibration procedure would be highly appealing for robotic US imaging system. Standard camera-to-robot procedures often involve laser trackers [20], coordinate measuring machines and depth cameras [21]. The average position error from robot to depth camera measurement was up to 3 mm and total calibration time ranged from 60 to 470 seconds [22].

The present work aims to introduce a fast, accurate and automatic framework for camera-to-robot calibration and robot US image calibration. The main contribution is the ability to automatically calibrate the US image in a short time with high accuracy. The proposed framework is different from the free hand calibration methods. This is inspired by the way how operators conduct US scans with complex free hand manipulation. It is the first paper combining robotic position control for US image calibration. The proposed methods were validated and demonstrated to quantify the reachable accuracy of the proposed framework with several 3D printed models.

This paper is organized as follows. Section II describes the proposed framework for camera-to-robot and robotic US calibration and related experiments. Section III presents and describes the experimental validation results of camera-to-robot calibration and US image calibration. Finally, Section IV concludes the work and indicates further work.

II. MATERIAL AND METHOD

The proposed framework aims to improve the efficiency and accuracy of robotic US calibration processes. Fig. 1 illustrates two main steps for the proposed framework, namely camera-to-robot calibration and US image calibration. Camera-to-robot calibration establishes a transformation between robot coordinate frame (robot frame) and 3D tracking system coordinate (camera frame). By doing so, the motions of robot end effector can be depicted in camera frame. The defined movement trajectories in camera frame can thus be transformed to robot frame. In this context, the pose of used phantom could be updated in robot frame as well. Obviously the robot arm can be programmed to perform scanning automatically. During scanning, US images and their corresponding spatial information can be stored. Then they can be processed simultaneously for US image calibration. In the end, robotic US based 3D reconstruction of a known object can be used for validating the outcome of calibration.

A. Experimental Setup

The proposed robotic US system consists of a lightweight robotic arm (KUKA Robot LWR, Augsburg, Germany), a US imaging system (Sonosite, FUJIFILM, USA) and an optical tracking system (FusionTrack 500, Atracsys, Switzerland).

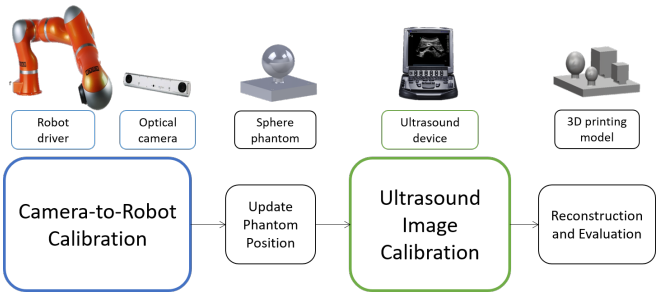

Fig. 1. Overview of the proposed framework for automatic robotic US calibration, including two main steps :camera-to-robot calibration and US image calibration.

The US system was operated with a 7.5MHz linear transducer. The settings of US device were chosen to cover the phantom with a clear image view, namely detection depth and time gain compensation (TGC). A frame grabber (Epiphan Systems Inc. Palo Alto, Canada) was used to stream the US images in 15Hz. A custom designed US probe holder was mounted onto the end effector of the robot by a fast tool changer. The new end effector was defined in Unified Robot Description Format (URDF) for following process. FusionTrack optical tracking system was operated at 335 Hz with 0.09 mm RMSE. To track the position and orientation of probe, an optical marker was attached on the holder. The calibration phantom, a 30 mm radius sphere, was designed and 3D printed by polylactide (PLA). In addition, a PC workstation (Intel i7, CPU @2.6 GHz, 64G RAM) was used for data acquisition and processing in Ubuntu 16.04. For robotic control middleware, Open Robot Control Software (Orocos version 2.9.0) was used for real-time control at 1 kHz. To control robot to conduct the required motions for US image calibration, eTasl (expressiongraph-based Task Specification Language), a constraint based task specification was utilized for robot position control [23]. The robot and the optical camera were connected to a workstation using direct Ethernet connection.

B. Camera-to-robot calibration

The accurate camera-to-robot calibration was based on point-to-point rigid registration. Fig. 2 showed a schematic overview of the different coordinate frames with the relevant transformations used throughout this work. The US probe pose in robot frame (${}^{US}_{R}T$) is represented by using robot forward kinematics from robot base to the new end effector defined in URDF. The unknown camera-to-robot transformation (${}^{R}_{C}T$) is necessary to match the two different coordinate frames, from camera frame (C) to robot frame (R). To obtain the pose of US probe in camera frame (${}^{US}_{C}T$), the established transformation can be found in Eq. 1.

$$ {}^{US}_{C}T = {}^{US}_{R}T \cdot {}^{R}_{C}T \tag{1} $$

Position control with velocity constraints used to control the robot new end effector, with given predefined target points in work space. An initial point was predefined in robot

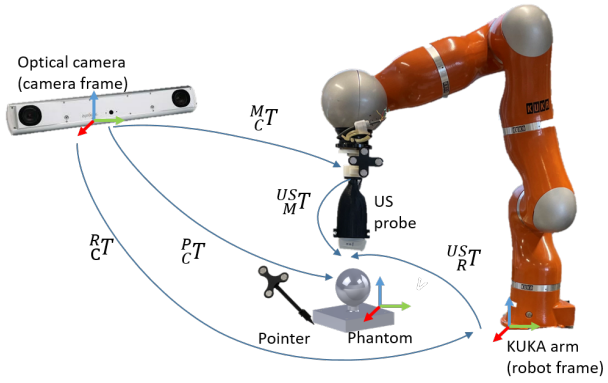

Fig. 2. Overview of involved transformations and coordinate frames in the setup. The notation $^{B}_{A}T$ is used to denote transformation from coordinate system A to B.

frame as a starting point for calibration procedure. Several equally distributed target points were generated around the initial point with a constant distance 100 mm along the directions of the xyz axes of robot frame. When robot end effector reached target point, the instantaneous marker position in camera frame was recorded. Once all defined target points were reached, camera-to-robot transformation matrix ($^{R}_{C}T = (^{R}_{C}r, ^{R}_{C}t)$) was computed by point-to-point rigid registration method [24]. The recorded point positions $U = u_i$ in camera frame were fit to the set of corresponding point positions $X = x_i$ in robot frame. The objective function which was minimized was:

$$f(^{R}_{C}r, ^{R}_{C}t) = \frac{1}{n}\sum_{i=1}^{n} \mid x_i - (^{R}_{C}ru_i + ^{R}_{C}t) \mid^2 \qquad (2)$$

We tested different number of target points (four points to seven points) to analyze their influence on the overall accuracy of camera-to-robot calibration. Each setting was repeated three times. For each experiment, the accuracy of camera-to-robot calibration is defined as $^{R}_{C}Error = f(^{R}_{C}r, ^{R}_{C}t)$. The mean and standard deviation of $^{R}_{C}Error$ were calculated and the operation time of each experiment was recorded. Results were summarized in Table II.

C. Automatic robot Ultrasound calibration

1) Robot motion planning and position control: The purpose of US image calibration is to establish correspondence between the marker frame and the US image frame. To realize the autonomous calibration procedure, the sphere phantom was registered in camera frame with an optical pointer in advance. Subsequently, by knowing the camera-to-robot transformation, the pose of the sphere phantom was updated to robot frame. In robot frame, the center of sphere was served as an anchor point for autonomous scanning. Position control with eTasl was implemented to keep the US probe always pointing to the anchor point. To acquire enough images and ensure a stable motion, the scanning speed of US probe tip was set as 2.5 mm/s for translation and 0.075 rad/s for rotation respectively. First, the US probe was aligned with sphere center in vertical direction as initial position. Then the probe started motion following scanning steps I to VII shown in table I. After finishing each step, the probe returned to initial position aligning with sphere center waiting for next motion. During scanning, US images were recorded with corresponding poses. Considering the working volume of optical camera, the attached marker should be detected during rotation and translation motions. For rotation, US probe was tilted between ± 30 degree angles while keeping the probe centerline passing through the sphere center. At the positions of ± 30 degree angles, US probe also translate along current pointing direction towards the sphere center in 10 mm, termed [-10, 0] motion range. Some illustration of the scanning motion were described in Fig. 3. During scanning, the center of sphere phantom was kept in sight of US image, while the optical marker and robot end effector track the different translations and rotations in the respective frame. This information will be used for further computation of calibration matrix.

TABLE I
SCANNING STEPS FOR US IMAGE CALIBRATION

Step	Motion type	Along axis	Motion range
I	Translation	phantom z axis	[-10 mm, 0]
II	Rotation	phantom x axis	[-30°, 30°]
III	Translation	pointing direction at $\pm 30°$	[-10 mm, 0]
IV	Rotation	phantom y axis	[-30°, 30°]
V	Translation	pointing direction at $\pm 30°$	[-10 mm, 0]
VI	Rotation	phantom z axis	[-30°, 30°]
VII	Translation	pointing direction at $\pm 30°$	[-10 mm, 0]

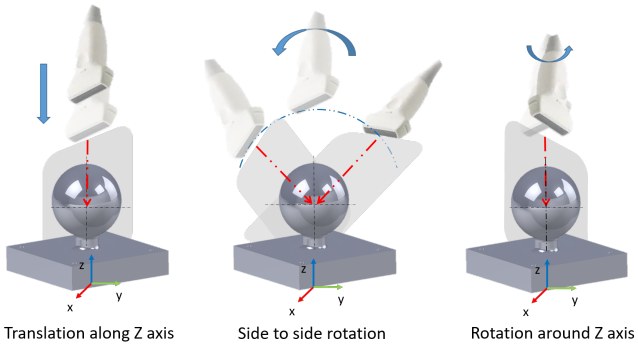

Fig. 3. Illustration of scanning motion examples over the sphere phantom. The red line is US probe centerline passing through sphere's center. The blue arrow indicates the direction of motion.

2) Image processing for US calibration: Considering the heavy workload of manual image segmentation, an automatic image segmentation method was developed to identify the sphere center point. Fig. 4 shows the workflow to automatically US image calibration. Firstly, a gaussian filter was applied to blur the image reducing white spike noise. Then the blurred image was binarized by thresholding. Morphological operator (closing) was used to remove small outliers and fill in the holes to obtain a continuous contour. Subsequently, the canny edge detection algorithm was applied to segment the sphere contour and only the upper contour was taken for computation. Least squares approach was applied to the

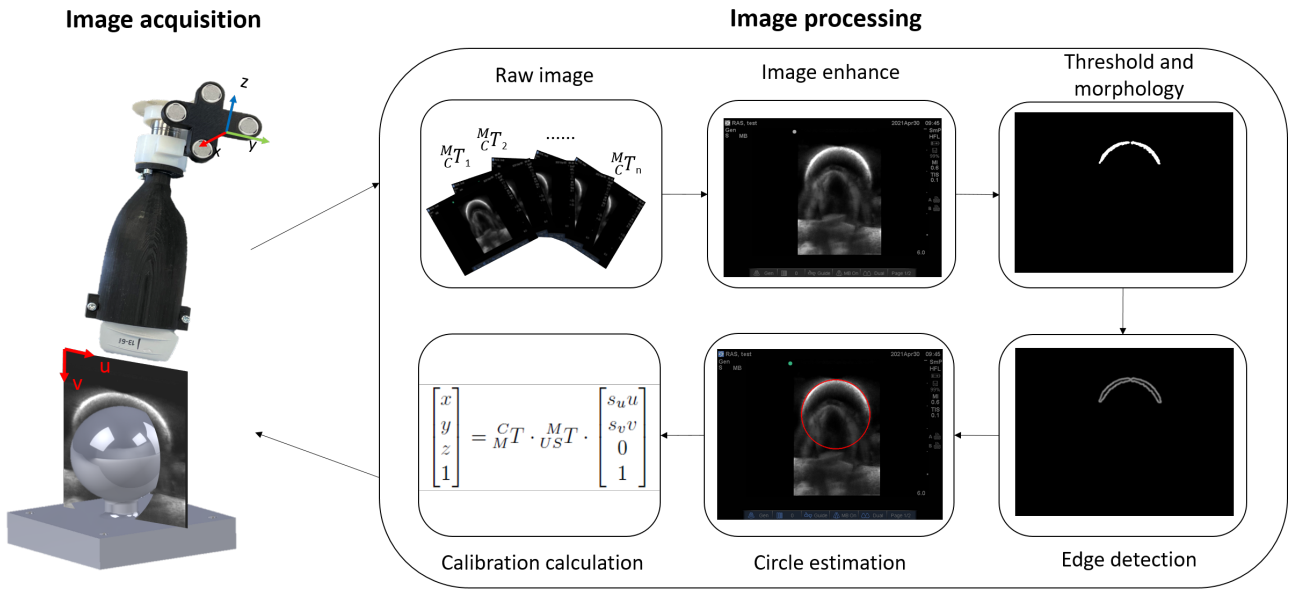

Fig. 4. Workflow of US image calibration. (Left) illustration of US image acquisition from custom designed sphere phantom; (Right) image processing procedures to automatically identify the sphere contour in 2D images and mapping of center point in 3D frame.

extracted sphere upper contour to estimate the center of circle with RANSAC to filter outliers. Finally, the center of sphere region was estimated in 2D ultrasound image, terms (u, v) in Fig. 4, and used as correspondence points to estimate the transformation matrices in calibration calculation. To reduce the computation time, the above mentioned process was developed in python script (3.7) and optimized with Numba featuring with Compute Unified Device Architecture (CUDA).

3) Ultrasound calibration method: To find the transformation from the marker coordinate to image coordinate, the following equation was set up. Capturing n images of the sphere phantom from various pose, the unknowns were computed by minimizing the following equation:

$$f(p) = \sum_{i=1}^{n} | \, {}^{p}_{C}T \cdot {}^{C}_{M}T \cdot {}^{M}_{US}T \cdot T_s \cdot p_i \, | \tag{3}$$

where ${}^{M}_{US}T$ is the homogeneous transformation matrix from the image frame (US) to the marker frame (M). ${}^{C}_{M}T$ describes the transformations from marker frame to camera frame. $p = [u, v, 0, 1]^T$ is the vector of estimated sphere center points in image frame while u and v denote the column and row pixel indices. T_s is the scaling factor matrix including s_u and s_v, the pixel to real distance in column and row directions of 2D US image respectively.

Furthermore, synchronization between 3D positioning data and image data was implemented to eliminate the sampling latency time. ROS framework with topic subscription was used for data acquisition. Once the incoming image message was received, the marker pose was checked and recorded in one callback.

4) Evaluation metrics: The performance of automatic image segmentation was evaluated, including scanning time, processing time and error metric. The error metric was defined as Euclidean distance between the actual sphere center and the calculated sphere center by transforming the identified 2D circle center to 3D positions with obtained transformation matrix. Five different experiments were conducted and the mean errors and standard deviations (Std. Dev.) of the calculated distances were shown in the table III.

D. Robotic 3D Ultrasound reconstruction

1) Point cloud reconstruction: Once both the camera-to-robot transformation and US image calibration were accomplished, the pixels in 2D US image thus could be transformed into the global coordinate system (i.e. camera frame). In reconstruction process, the pixels of segmented contour (u, v) were converted into point cloud (x, y, z) in the camera frame shown in Eq 4.

$$\begin{bmatrix} x \\ y \\ z \\ 1 \end{bmatrix} = {}^{C}_{M}T \cdot {}^{M}_{US}T \cdot \begin{bmatrix} s_u u \\ s_v v \\ 0 \\ 1 \end{bmatrix} \tag{4}$$

The US image sequences and corresponding poses were transmitted simultaneously to reconstruction algorithm to generate 3D points. In previous researches, the interpolation method was developed to render volume. But this paper focused on geometry features (for example the spinal process and transverse process) rather than entire anatomical volume. To visualize those features, the Visualization Toolkit (VTK) (https://https:/vtk.org/) was used for developing a custom program for 3D visualization.

2) Evaluation of model reconstruction: The accuracy of the US image calibration was verified by reconstructing a 3D printed mock-up model (sphere-cube model) with known geometry. The mock-up model consisted of two cubes and two spheres with lengths of 20 mm and 30 mm, respectively,

shown in Fig. 5. The validation mock-up model was placed stationary in a water bath for scanning. The probe was moved by robot controller along a predefined trajectory to record data covering both spheres and cubes. During robotic scanning, the US probe was kept at a constant orientation which was perpendicular to the bottom surface of the mock-up model. For evaluation, the reconstructed point cloud was registered to its CAD model by using ICP registration. This validation shows the accuracy of US image calibration with 3D representation error by representing size and shape of the scanned model.

A second validation assessed whether the reconstructed point cloud locates at the actual 3D position of the phantom (i.e. the ground truth position of the phantom in camera frame), termed 3D localization error. The ground truth position of the phantom was obtained by optical pointer prior to each experiment. Any movement of the phantom was avoided during experiment. The results were shown in Table IV. Moreover, a 3D printed spine model was scanned and reconstructed to demonstrate feasibility of the proposed method of reconstructing a complex geometry. The 3D representation error was shown in Fig. 6

III. RESULTS

A. Result of camera-to-robot calibration

The results of camera-to-robot calibration are shown in the table II for different numbers of target points (from four points to seven points). The results showed that the mean error decreased with the number of target points. When there were 6 target points, the mean error was 0.17 mm. Meanwhile, it is reasonable to find that the total operation time increased as more target points were used. The average operation time was 33, 39, 48, and 55 seconds for 4, 5, 6 and 7 points, respectively.

TABLE II

QUANTITATIVE MEASUREMENTS OF CAMERA-TO-ROBOT CALIBRATION WITH VARIOUS NUMBER OF TARGET POINTS.

Number of target points	4	5	6	7
Experiment 1	0.51	0.30	0.23	0.38
Experiment 2	1.09	0.53	0.14	0.28
Experiment 3	0.95	0.23	0.13	0.18
Mean error (mm)	0.85	0.35	0.17	0.28
Std. Dev. (mm)	0.30	0.16	0.05	0.10
Average time (s)	33	39	47	55

B. Result of ultrasound image calibration

Five sets of experiment were conducted to evaluate the performance of US image calibration shown in Table III. The mean error ranged from 1.95 to 3.97 mm among the testings, while standard deviations were between 0.77 and 0.95 mm. The average processing time for each image segmentation is about 0.025 seconds and the average number of acquired US image is 1122. The average robot scanning time is 152 seconds while the average image processing time is 25.8 seconds.

TABLE III

EXPERIMENTAL RESULTS OF US IMAGE CALIBRATION

Exp. number	Exp. 1	Exp. 2	Exp. 3	Exp. 4	Exp. 5
Number of images	1002	1053	1090	1224	1241
Scanning time (s)	141	146	150	161	164
Processing time (s)	23.5	24.1	24.7	27.9	28.7
Mean error (mm)	1.95	2.29	2.09	3.97	3.06
Std. Dev. (mm)	0.84	0.78	0.95	0.95	0.77

C. Result of 3D model reconstruction

The sphere-cube model was reconstructed and validated. To assess 3D representation error, as shown in Fig. 5, the reconstructed point clouds were superimposed and matched with CAD model after ICP registration. As the US probe followed a straight line and kept perpendicular to the bottom surface of the model, only the upper surfaces of the model were generated completely. Overall, the RMSE of ICP registration between reconstructed point cloud to the CAD model were 0.74, 1.21 and 1.68 mm for three repeated experiments, respectively. The mean representation error ranged from 0.75 to 1.30 mm. These accurate alignments indicated good capability of representing the geometries with different shapes and sizes.

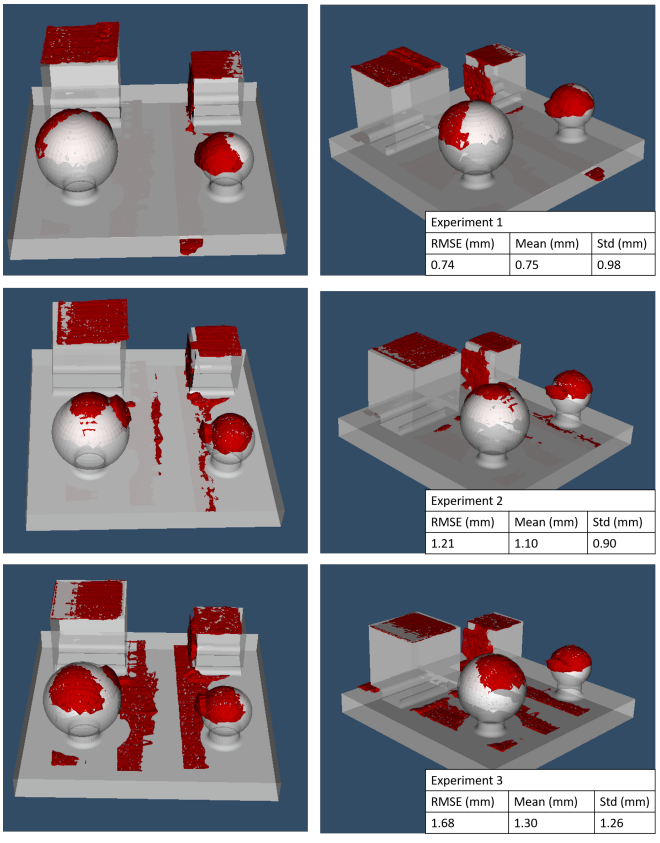

Fig. 5. Illustrations and quantitative measurements of 3D representation error from three experiments. The red model is the reconstructed point cloud, while the white model is the respective CAD model. (Left) top view of the results; (Right) side view of the results with error tables.

To assess 3D localization error (i.e. if the 3D US recon-

struction could produce a point cloud at the correct location in actual 3D space), the 3D reconstructed point clouds were compared with the ground truth location of the phantom that was derived by 3D optical pointer. The mean localization errors for the reconstruction result to the ground truth were ranged from 1.11 to 1.41 mm in Table IV.

TABLE IV
3D LOCALIZATION ERRORS OF THE RECONSTRUCTED POINT CLOUD WITH THE CORRESPONDING GROUND TRUTH

Exp. number	Exp. 1	Exp. 2	Exp. 3
RMSE (mm)	2.00	1.18	1.22
Mean error (mm)	1.41	1.34	1.11
Std. Dev. (mm)	1.05	1.04	0.87

The reconstruction result of a lumbar vertebrae is shown in Fig. 6. The red surface meshes were generated from a point cloud and visualized as surface mesh with spine model in the VTK viewer. The spinal process and transverse process was placed on the CAD model surface accurately. The mean 3D representation error was 1.00 mm compared to this CAD model.

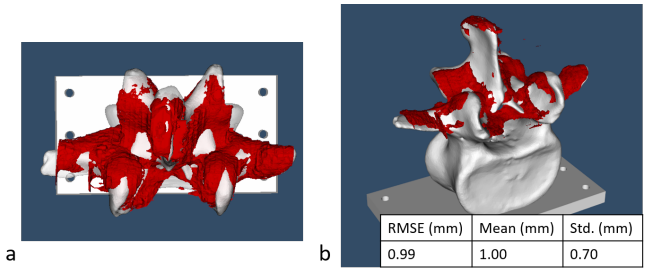

Fig. 6. Automatic 3D reconstruction result (red) compared to the spine model obtained from CT scan (white) after ICP. (a) top view of reconstruction result; (b) left side view of the reconstruction result.

IV. DISCUSSION AND CONCLUSIONS

US image calibration is an important step to ensure a high quality 3D US reconstruction. In this paper, we combined three important steps for robotic ultrasound systems, which integrates the camera-to-robot calibration, robotic ultrasound image calibration and robotic 3D ultrasound reconstruction into a unified pipeline for robotic US system. The proposed framework could realize a fast, high precision camera-to-robot calibration and robotic US image calibration and eventually achieve robotic ultrasound scanning for 3D reconstruction with high accuracy. To the best of authors' knowledge, it is the first time to assemble all necessary steps for robotic ultrasound system. The proposed framework also has been validated to provide high accuracy. The entire duration of full calibration procedures does not exceed 4 minutes with less than 1.3 mm error, which has great potential to facilitate the advancement of automatic robot ultrasound scanning.

In this paper, a camera-to-robot calibration method was presented and developed using the point-to-point registration algorithm. The experimental results showed that the calibration accuracy increased with the number of target point while leading to longer manipulation time. For 6 target points, the mean error can reach 0.17 mm over three repeated experiments and average operation time is 47 seconds. This calibration error is much smaller than previous result which the camera-robot calibration error was up to 4 mm [25]. Besides, the operating time of proposed method is also shorter while the total procedure took about 40 min in Ozguner's research. In recent researches, depth camera was also widely integrated with robotic system as visual serving for calibration, such as the Roberti's research [26]. The 3D calibration result of camera and robotic arms can also reach an accuracy below 1 mm.

This paper mainly aims to improve the performance of US image calibration, especially in the robotic fashion. Compared to different US calibration phantoms, the sphere phantom was chosen since the sphere shape enables a rapid automatic image segmentation for robotic US scanning without manual intervention. Besides, position controlled US scanning ensures a sufficiently diverse range of probe poses avoiding the under-determined results when estimate the sphere center. It is also more stable while keeping a good alignment between US probe and the sphere center comparing to free hand manipulation. Moreover, the segmentation time for each image is 0.025 seconds. In contrast, the conventional manual image segmentation and post processing usually last several minutes [27]. Since the US image processing time has been noticeably shortened, more images could be collected from different poses to improve the calibration accuracy. Therefore, the proposed automatic US image calibration framework has potential applications in robotic assisted system thanks to its feasibility and stability.

In the experimental part, the proposed framework is proved to be feasible. The validation results show that the reconstructed point clouds could accurately outline the geometric features comparing with the respective geometry model via ICP registration. In previous studies, most of results only focused on the accuracy of 3D representation error and verified geometry features rather than the 3D localization error [28]. The 3D localization result is essential to display the reconstructed model to surgeon in medical scenarios interacting with other surgical instruments. Using optical pointer and registration algorithm, the geometry model is transformed into camera frame that served as ground truth. The mean 3D localization error was 1.29 mm for three repeated experiments from reconstruction point clouds to ground truth model. The proposed methods in this paper not only improve the precision of geometric feature reconstruction but also quantify the accuracy of the reconstruction result in terms of the 3D localization error.

Robotic US imaging is an emerging technology that reduces workload and empowers the optimal probe scanning rather than free hand manipulation. A fast, automatic and reliable robot US image calibration method would then facilitate the deployment and implementation of robotic US systems in practice and therefore enhance the ultimate accuracy and precision of robot-assisted applications.

REFERENCES

[1] D. L. Miller, N. B. Smith, M. R. Bailey, G. J. Czarnota, K. Hynynen, I. R. S. Makin, and B. C. of the American Institute of Ultrasound in Medicine, "Overview of therapeutic ultrasound applications and safety considerations," Journal of ultrasound in medicine, vol. 31, no. 4, pp.623–634, 2012.

[2] K. Niu, T. Anijs, V. Sluiter, J. Homminga, A. Sprengers, M. A. Marra, and N. Verdonschot, "In situ comparison of a-mode ultrasound tracking system and skin-mounted markers for measuring kinematics of the lower extremity," Journal of biomechanics, vol. 72, pp. 134–143, 2018.

[3] R. Li, K. Niu, D. Wu, and E. Vander Poorten, "A framework of realtime freehand ultrasound reconstruction based on deep learning for spine surgery," in 10th Conference on New Technologies for Computer and Robot Assisted Surgery, Location: Barcelona, Spain, 2020.

[4] M. R. Morgan, J. S. Broder, J. J. Dahl, and C. D. Herickhoff, "Versatile low-cost volumetric 3-d ultrasound platform for existing clinical 2-d systems," IEEE Trans. Med. Imaging, vol. 37, no. 10, p. 2248–2256, 2018.

[5] Q. Huang, B. Wu, J. Lan, and X. Li, "Fully automatic threedimensional ultrasound imaging based on conventional b-scan," IEEE Trans. Biomed. Circuits Syst, vol. 12, p. 426–436, 2018.

[6] K. Niu, J. Homminga, V. Sluiter, A. Sprengers, and N. Verdonschot, "Measuring relative positions and orientations of the tibia with respect to the femur using one-channel 3d-tracked a-mode ultrasound tracking system: A cadaveric study" Medical engineering & physics, vol. 57, pp. 61–68, 2018.

[7] L. Mercier, T. Lango, F. Lindseth, and D. L. Collins, "A review of calibration techniques for freehand 3-d ultrasound systems," Ultrasound Med. Biol., vol. 31, no. 4, p. 449–471, 2005

[8] D. P. adn Bashein G and e. a. Hodges T, "3d ultrasonic image feature localization based on magnetic scanhead tracking: In vitro calibration and validation," Ultrasound Med Biol, vol. 20, p.923–936, 1994.

[9] B. Brendel, S. Winter, and H. Ermert, "A simple and accurate calibration method for 3d freehand ultrasound," Biomedizinische Technik BMT, 2004.

[10] S. Meairs, J. Beyer, and M. Hennerici, "Reconstruction and visualization of irregularly sampled three- and four-dimensional ultrasound data for cerebrovascular applications," Ultrasound Med. Biol., vol. 26, p. 263–272, 2000.

[11] R. W. Prager, R. N. Rohling, A. H. Gee, and L. Berman, "Rapid calibration for 3-d freehand ultrasound," Ultrasound in Medicine Biology, vol. 24, no. 6, p. 855–869, 1998.

[12] R. A. Brown, "A stereotactic head frame for use with ct body scanners," Invest. Radiol., vol. 14, no. 4, p. 300–304, 1979.

[13] PW. Hsu, R. W. Prager, N. E. Houghton, A. H. Gee, and G. M. Treece, "Accurate fiducial location for freehand 3d ultrasound calibration,"

[21] R. A. Boby and S. K. Saha, "Single image based camera calibration and pose estimation of the end-effector of of a robot," in IEEE International Conference on Robotics and Automation, 2016.

in Proceedings of SPIE - The International Society for Optical Engineering, vol. 6513, 2007, p. 651315.

[14] A. S. Savoia, G. Caliano, G. Matrone, A. Ramalli, E. Boni, and P. Tortoli, "Nonlinear ultrasound imaging experiments using a cmut probe," 2016 IEEE International Ultrasonics Symposium (IUS), 2016.

[15] P.-W. Hsu, R. W. Prager, A. H. Gee, and G. M. Treece, "Freehand 3d ultrasound calibration: A review," Advanced Imaging in Biology and Medicine, p. 47–84, 2009.

[16] F. Lindseth, G. A. Tangen, T. Langø, , and J. Bang, "Probe calibration for freehand 3-d ultrasound," Ultrasound Med. Biol., vol. 29, no. 11, p. 1607–1623, 2003.

[17] M.-A. Vitrani and G. Morel, "Hand-eye self-calibration of an ultrasound image-based robotic system," in IEEE RSJ International Conference on Intelligent Robots and Systems, 2008.

[18] Q. Huang, J. Lan, and X. Li, "Robotic arm based automatic ultrasound scanning for three-dimensional imaging," IEEE Transactions on Industrial Informatics, vol. 15, p. 1173–1182, 2019.

[19] G. Ning, X. Zhang, and H. Liao, "Autonomic robotic ultrasound imaging system based on reinforcement learning," IEEE Trans. Biomed.Eng., pp. 1–1, 2021.

[20] J. Conte, A. C. Majarena, S. Aguado, R. Acero, and J. Santolaria, "Calibration strategies of laser trackers based on network measurements," The International Journal of Advanced Manufacturing Technology, vol. 83, no. 5–8, p. 1161–1170, 2016.

[22] J. Miseikis, K. Glette, O. J. Elle, and J. Torresen, "Automatic calibration of a robot manipulator and multi 3d camera system," in IEEE SICE International Symposium on System Integration, 2016.

[23] E. Aertbelien and J. D. Schutter, "etasl/etc: A constraint-based task specification language and robot controller using expression graphs," in International Conference on Intelligent Robots and Systems, 2014.

[24] K. Niu, J. Homminga, V. I. Sluiter, A. Sprengers, and N. Verdonschot, "Feasibility of a-mode ultrasound based intraoperative registration in computer-aided orthopedic surgery: a simulation and experimental study," Plos One, 2018.

[25] O. Ozguner et al., "Camera-robot calibration for the da vinci robotic surgery system," IEEE Transactions on Automation Science and Engineering, vol. 17, p. 2154–2161, 2020.

[26] A. Roberti, N. Piccinelli, D. Meli, R. Muradore, and P. Fiorini, "Improving Rigid 3-D Calibration for Robotic Surgery," IEEE Transactions on Medical Robotics and Bionics, vol. 2, no. 4. pp. 569–573, 2020. doi: 10.1109/tmrb.2020.3033670.

[27] F. Rousseau, P. Hellier, M. M. J. Letteboer, W. J. Niessen, and C. Barillot, "Quantitative evaluation of three calibration methods for 3-d freehand ultrasound," IEEE Trans. Med. Imaging, vol. 25, p.1492–1501, 2006.

[28] F. Cenni, S.-H. S. D. Monari, E. Aertbelien, K. Desloovere, and ¨H. Bruyninckx, "Efficient image based method using water-filled balloons for improving probe spatial calibration in 3d freehand ultrasonography," Ultrasonics journal, vol. 94, p. 124–130, 2019.